Turbulence kinetic energy in turbulent flows through square ducts with rib-roughened walls

Masafumi Hirota
Department of Mechanical Engineering, Nagoya University, Nagoya, Japan

Hajime Yokosawa
College of General Education, Nagoya University, Nagoya, Japan

Hideomi Fujita
Department of Mechanical Engineering, Nagoya University, Nagoya, Japan

Turbulence kinetic energy production and convection were examined in detail for the turbulent flows through various square ducts. The following ducts were used: a smooth duct, a duct with one wall roughened, and a duct with two facing walls roughened. Rough walls were produced by gluing square ribs to a smooth surface repeatedly. By the examinations the turbulent shear stresses were found to play the most important role in the production of the turbulence kinetic energy. Near the rough walls the turbulent normal stresses also have strong influences on the energy production, although their contributions are either positive or negative, depending on the relative streamwise locations with respect to a rib roughness element. The amount of turbulence energy convected by secondary flow is considerably smaller than that of the energy produced. The secondary flow has little influence on the balance of turbulence kinetic energy in the tested ducts.

Keywords: turbulent flow; duct flow; secondary flow of the second kind; turbulence kinetic energy; square duct; rib-roughness element

Introduction

In an attempt to enhance convective heat transfer in turbulent flows through ducts, the use of repeated rib-roughness elements has been given considerable attention.[1] The flows in ducts with ribbed walls, however, are so complicated that few results have been presented for detailed turbulence characteristics in the ducts.[2] In line with this, the present authors have reported experimentally obtained characteristics of the turbulent flows through square ducts with one or more rib-roughened walls.[3–6] The rough wall enhances the generation of turbulence, and consequently it exerts great influences on the turbulence energy distributions in the ducts. Thus, it is significant to examine turbulence energy balances in the rough ducts and to compare them with those in the smooth-walled duct for further investigation of the effects of rough walls on the turbulence structures in the ducts. As for a rectangular duct roughened homogeneously by plastic grains, detailed characteristics of the turbulence energy balance have been examined in an earlier experiment.[7,8] These results, however, would not apply to the rib-roughened ducts, because ribs bring about extreme inhomogeneous flow behavior in the direction of primary flow.[2] To the authors' knowledge, very few results have been presented for turbulence energy balances in rectangular ducts with ribbed walls.

This paper presents the results of the examination of the turbulence kinetic energy balance based on detailed measurements of the flows in three square ducts: a smooth duct (duct A), a duct with one rib-roughened wall (duct B), and a duct with two facing ribbed walls (duct C). The present results include the following:

(1) turbulence energy production caused by turbulent shear and cross-planar normal stresses;
(2) turbulence energy convected by secondary flow of the second kind,[9] which is inherent to turbulent flows in straight noncircular ducts;
(3) turbulence energy production caused by streamwise gradient of the primary flow velocity;
(4) differences between energy balances obtained atop a rib and that obtained downstream of the rib.

Address reprint requests to Dr. Hirota at the Department of Mechanical Engineering, Nagoya University, Furo-cho, Chikusa-ku, Nagoya, 464–01, Japan.

Received 11 May 1990; accepted 6 June 1991

Turbulence energy transport equation

Transport equation for turbulence energy, $k = (\overline{u_1^2} + \overline{u_2^2} + \overline{u_3^2})/2$ reads[10]

$$\frac{Dk}{Dt} + \frac{\partial}{\partial x_i}\overline{u_i\left(\frac{p}{\rho} + \frac{u_j u_j}{2}\right)} + \overline{u_i u_j}\frac{\partial U_j}{\partial x_i} - \nu\frac{\partial}{\partial x_i}\overline{u_j\left(\frac{\partial u_i}{\partial x_j} + \frac{\partial u_j}{\partial x_i}\right)} + \nu\overline{\left(\frac{\partial u_i}{\partial x_j} + \frac{\partial u_j}{\partial x_i}\right)\frac{\partial u_j}{\partial x_i}} = 0, \qquad (i, j = 1, 2, 3) \tag{1}$$

Among the terms in Equation 1, contribution of the terms of energy production caused by turbulent shear stress, $\overline{u_2 u_3}(\partial U_2/\partial x_3 + \partial U_3/\partial x_2)$, is estimated to be negligibly small. Since ribs are used to make up rough ducts, the flows repeat separation and reattachment near the ribs. It follows that $\partial U_1/\partial x_1$ is not equal to zero locally even when the flow is fully developed globally. Accordingly, when the energy balance is examined, the contribution of each term related to $\partial/\partial x_1$ should be taken into account. An accurate estimation of these terms including the convective energy transport term, $U_1\,\partial k/\partial x_1$,

however, was so difficult that only the energy production by normal stress, $\overline{u_1^2}\,\partial U_1/\partial x_1$, was taken into account. By applying boundary-layer approximations, $U_1\,\partial k/\partial x_1$ can be estimated to be of the same order of magnitude as the terms of energy convection caused by the secondary flow.

After applying the above approximations, Equation 1 becomes

$$U_2\frac{\partial k}{\partial x_2}+U_3\frac{\partial k}{\partial x_3}+\overline{u_1u_2}\frac{\partial U_1}{\partial x_2}+\overline{u_1u_3}\frac{\partial U_1}{\partial x_3}+\overline{u_1^2}\frac{\partial U_1}{\partial x_1}+\overline{u_2^2}\frac{\partial U_2}{\partial x_2}+\overline{u_3^2}\frac{\partial U_3}{\partial x_3}+\varepsilon+D_f=0 \quad (2)$$

where ε stands for the dissipation term and D_f for the diffusion term. In the analysis, Equation 2 is made nondimensional with the use of the hydraulic diameter of ducts, D, and the maximum velocity in the measurement cross section, U_S. Examined terms are enumerated below:

Convection:

$$C=\left(U_2\frac{\partial k}{\partial x_2}+U_3\frac{\partial k}{\partial x_3}\right)\frac{D}{U_S^3} \quad (3a)$$

Production caused by turbulent shear stresses:

$$P_S=\left(\overline{u_1u_2}\frac{\partial U_1}{\partial x_2}+\overline{u_1u_3}\frac{\partial U_1}{\partial x_3}\right)\frac{D}{U_S^3} \quad (3b)$$

Production caused by turbulent normal stresses:

$$P_N=\left(\overline{u_1^2}\frac{\partial U_1}{\partial x_1}+\overline{u_2^2}\frac{\partial U_2}{\partial x_2}+\overline{u_3^2}\frac{\partial U_3}{\partial x_3}\right)\frac{D}{U_S^3} \quad (3c)$$

Dissipation and diffusion:

$$R=(\varepsilon+D_f)\frac{D}{U_S^3} \quad (3d)$$

The sum of dissipation and diffusion was taken as the closing entry, because neither dissipation nor diffusion could be measured accurately in our experiments.

Experimental apparatus and method

The flow system of this experiment is the same as that used in an experiment reported earlier.[5] The test square ducts, whose side length is 50 mm ($= D = 2B$), are straight and 4,500 mm in length. The three types of square ducts shown in Figure 1 were used in the experiments. In the rest of the paper, a smooth-walled duct is referred to as duct A, a duct with one rough wall as duct B, and a duct with two facing rough walls as duct C. The rough wall was produced by 1-mm square-sectioned ribs glued to the surface at 10-mm intervals and oriented transverse to the primary flow (Figure 2).

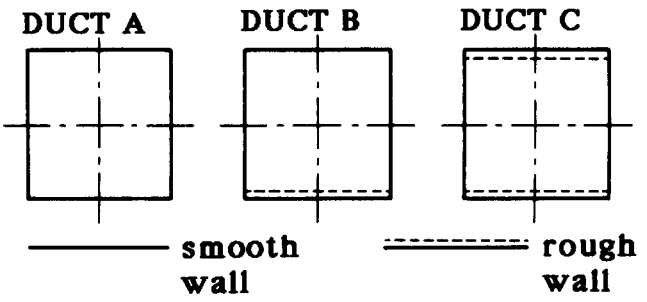

Figure 1 Tested ducts

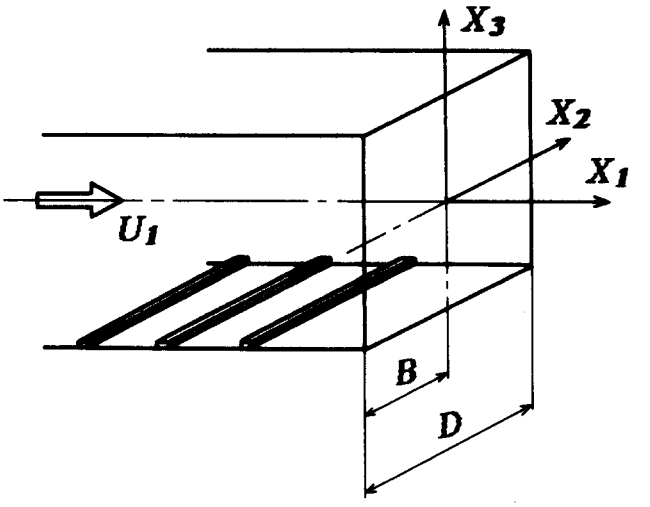

Figure 2 Coordinate system

The coordinate system is shown in Figure 2. Components of the mean velocity are designated as U_1, U_2, and U_3, and those of fluctuation velocity as u_1, u_2, and u_3, respectively. Rough walls are perpendicular to the x_3 axis.

The analysis is mainly based on the measurements obtained at station I, which is the section located 5 mm downstream of the furthest downstream rib (89.8 D from duct entrance). This cross section is located in the immediate vicinity of the flow reattachment point[11] (Figure 3), and corresponds to the station

Notation

$B = D/2$	Half length of a side of a square duct
C	Energy convection by the secondary currents (Equation 3a)
D	Length of a side of square duct or hydraulic diameter of duct
k	Turbulence kinetic energy $(= (\overline{u_1^2}+\overline{u_2^2}+\overline{u_3^2})/2)$
P	Energy production $(= (P_S + P_N))$
P_N	Energy production caused by turbulent normal stresses (Equation 3c)
P_S	Energy production caused by turbulent shear stresses (Equation 3b)
$\mathrm{Re} = UD/\nu$	Reynolds number
u_1, u_2, u_3	Fluctuation velocities in x_1-, x_2-, and x_3-directions, respectively
$\overline{u_1u_2}, \overline{u_1u_3}$	Turbulent shear stresses in x_2- and x_3-directions, respectively
U	Bulk mean velocity
U_1, U_2, U_3	Mean velocities in x_1-, x_2-, and x_3-directions, respectively
U_S	Maximum velocity in the measurement cross section
x_1, x_2, x_3	Orthogonal coordinate

Greek symbols

ε	Dissipation term in Equation 2
ν	Kinematic viscosity of fluid

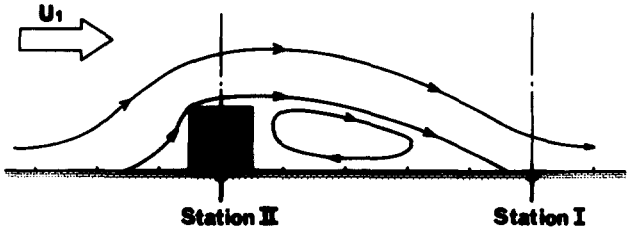

Figure 3 Streamlines near the rough wall and measurement stations

located midway between two successive ribs. The primary flow velocity at the center of the duct's cross section attains a constant value about 50 D downstream from the duct entrance. The flow at the measuring cross section can therefore be regarded as fully developed globally. However, in the neighborhood of the rough wall, flow repeats separation and reattachment, causing changes in primary velocity in the streamwise direction.[11,12] In order to determine differences in the energy balances that are brought about by the difference in the relative locations of measuring cross sections with respect to the roughness element, additional measurements were carried out at the cross section running atop the rib furthest downstream (89.7 D from duct entrance, named station II). The locations of station I and station II relative to the rib and a sketch of streamlines near the rough wall[11,12] are depicted in Figure 3.

Flow measurements were conducted keeping Reynolds number Re ($=UD/\nu$) at 6.5×10^4. Velocities and stresses were measured by means of hot-wire anemometers with two X-wire probes, mirror images of each other, for eliminating errors due to velocity gradient.[13] The velocity gradients included in the production terms in Equation 2 were obtained by direct numerical differentiation using the finite difference method. The least interval of the differential grid is 0.25 mm.

As described previously, station I was set 5 mm downstream of the furthest downstream rib for the convenience of inserting the X-wire probes. Since there are no further ribs beyond station I, the flow behavior downstream of this station changes toward that in the smooth-walled duct. Hence, in order to investigate whether the flow behavior at station I is periodic like that observed at a station between two ribs, the axial velocities around the furthest downstream rib were measured in detail. This preliminary experiment proved that the flow behavior at station I is exactly the same as that observed midway between two successive ribs and is representative of that observed midway between ribs.

The uncertainties involved in the measured values were estimated as follows: U_1, ± 1.4 percent; U_2 and U_3; ± 6.0 percent; $\overline{u_1^2}$, ± 2.4 percent; $\overline{u_2^2}$ and $\overline{u_3^2}$, ± 8.6 percent; and $\overline{u_1 u_2}$ and $\overline{u_1 u_3}$, ± 4.9 percent.

Results and discussion

Energy production

Contours of turbulence energy production, $(P_S + P_N)$, are shown in Figures 4–6 together with the contours of turbulence energy k. Since the contour maps obtained in each duct were extremely symmetrical with respect to the planes of geometric symmetry of the duct, the results in half of the cross section are depicted. The results of the rough duct shown in this section and in the next two sections are based on the measurements at station I (the cross section downstream of the rib). The broken lines, drawn in Figures 5 and 6 for the rough ducts, show the height of roughness elements.

In each duct, the contours of $(P_S + P_N)$ and k are much alike. In Figure 4 for duct A, contour lines of both $(P_S + P_N)$ and k for smaller values jut out toward corners of the duct. And near each corner, the values both of $(P_S + P_N)$ and k increase rapidly as the corner is approached. This shows that energy production caused by shear and normal stresses has a great effect on the distribution of k. The reason for rapid increase in $(P_S + P_N)$ and k near the corners can be illustrated as follows. Secondary currents transport high momentum fluid lumps from the core toward the corners. This gives rise to steep velocity gradients near the corners, and large turbulent shear stresses caused by steep velocity gradient contribute to a large energy production. As a result, distortions in contour lines of k are more pronounced than those in contour lines for primary flow velocity, U_1.[4,6]

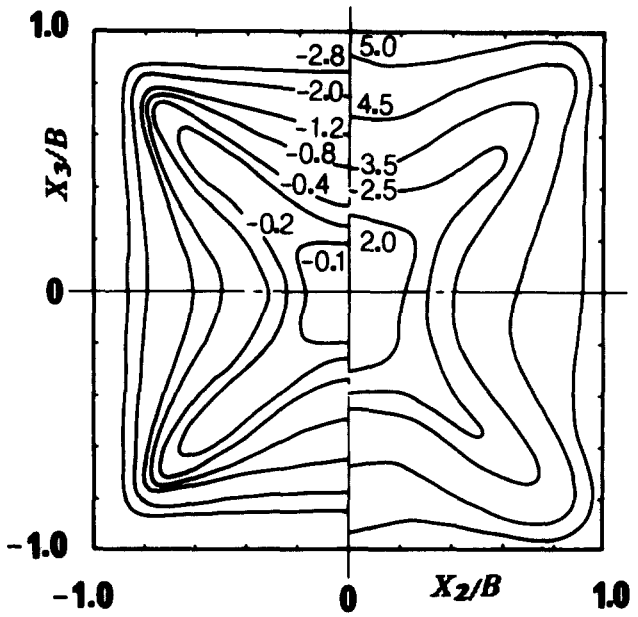

Figure 4 Turbulence energy production $(P_S + P_N) \times 10^3$ (left) and turbulence energy $k/U_S^2 \times 10^3$ (right) for duct A

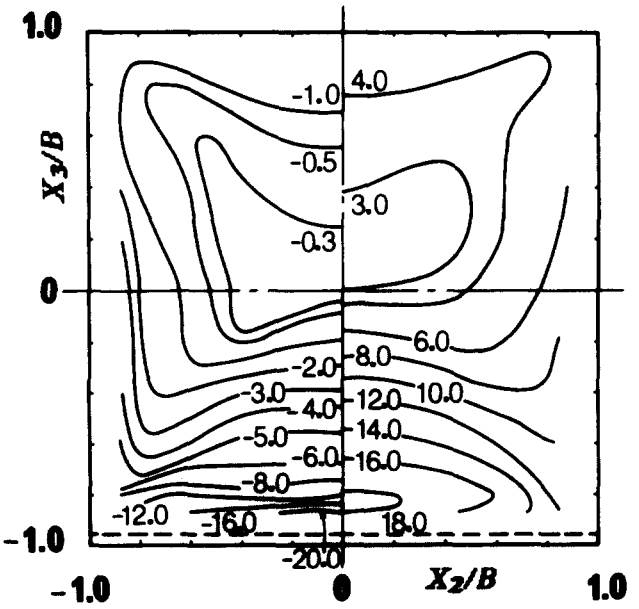

Figure 5 Turbulence energy production $(P_S + P_N) \times 10^3$ (left) and turbulence energy $k/U_S^2 \times 10^3$ (right) for duct B

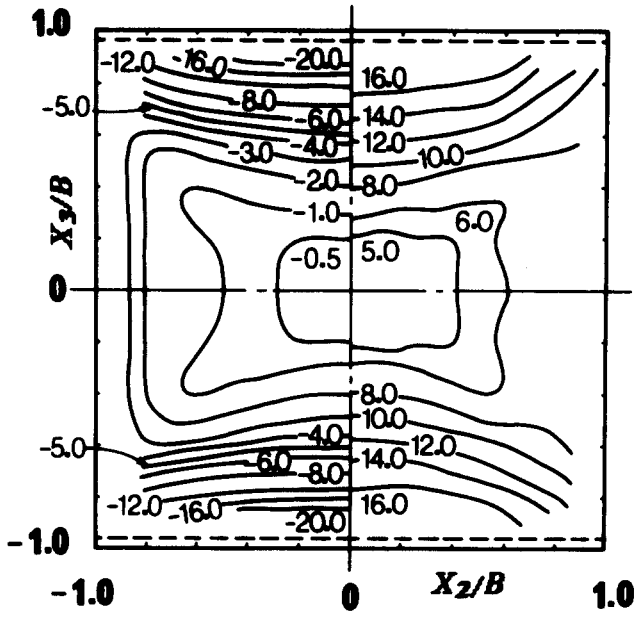

Figure 6 Turbulence energy production $(P_S + P_N) \times 10^3$ (left) and turbulence energy $k/U_S^2 \times 10^3$ (right) for duct C

In Figure 5, contour maps of $(P_S + P_N)$ and k are shown for duct B. In the upper corners composed by upper and side smooth walls, contour lines jut out toward corners just as has been observed in duct A. In the vicinity of the rough wall, the magnitude of the value of $(P_S + P_N)$ is several times larger than that measured in duct A, and the high level of $(P_S + P_N)$ corresponds to the high level of k in this region. In addition to this, the distribution of $(P_S + P_N)$ near the rough wall agrees well quantitatively with that for duct C, shown in Figure 6. The same is true for the distribution of k. As expected from these results, in the present study, any quantities obtained near the rough wall in duct B were quite similar to those in duct C. It follows that the results of duct B are representative of those near the rib-roughened wall. Therefore, in the following sections, presentation of the results obtained in duct C are omitted, and the results obtained in duct A and duct B are examined in detail.

Turbulence energy balance

Figures 7 and 8 show the energy balances based on Equation 2 and examined along the axis of symmetry of each duct. A term that is negative in sign corresponds to a gain in energy, and a term that is positive in sign corresponds to a loss in energy. The broken line in Figure 8 corresponds to the height of ribs.

In duct A, as shown in Figure 7, the production caused by normal stresses, P_N, is much smaller than the production caused by shear stresses, P_S. P_S contributes to the production of the streamwise fluctuating velocity component u_1. Therefore, it is speculated that in the smooth duct the turbulence kinetic energy produced by P_S is initially stored in $\overline{u_1^2}$, and then some portion of it is redistributed to the other components $\overline{u_2^2}$ and $\overline{u_3^2}$. The energy convection is almost equal to zero on the x_3 axis.

P_S for duct B, as can be noticed in Figure 8, is a large negative value (gain in energy) near the rough wall, almost zero near the center of the duct and negative again near the upper smooth wall. The magnitude of P_S near the upper smooth wall is much smaller than that near the rough wall, and it is almost of the same level as that observed in the corresponding region in duct A. The large magnitude of P_S near the rough wall of duct B is explained as follows. Near the ribs, the free shear layer is formed between the primary flow and the recirculating flow in the separation bubble (Figure 3). This shear layer produces vorticity of high level in the x_2-direction, which contributes to a large magnitude of turbulent shear stress $\overline{u_1 u_3}$. Moreover, the gradient of U_1 in the x_3-direction, $\partial U_1/\partial x_3$, is also large near the rough

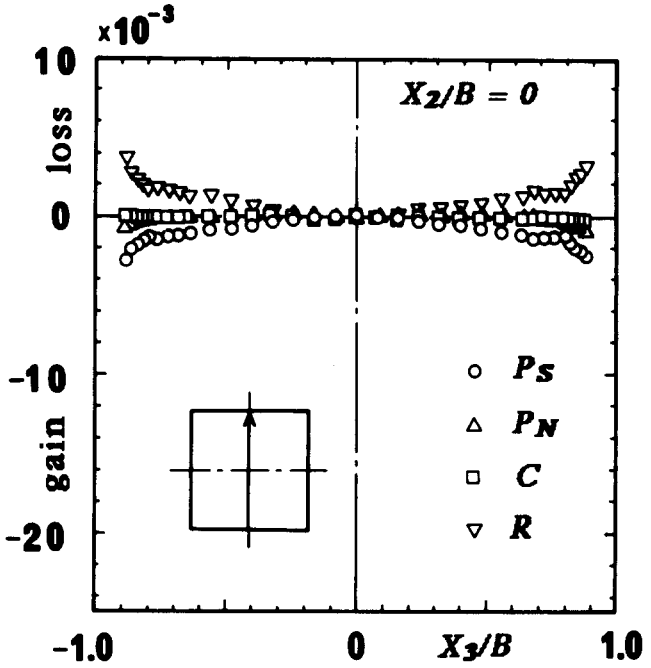

Figure 7 Energy balance for duct A

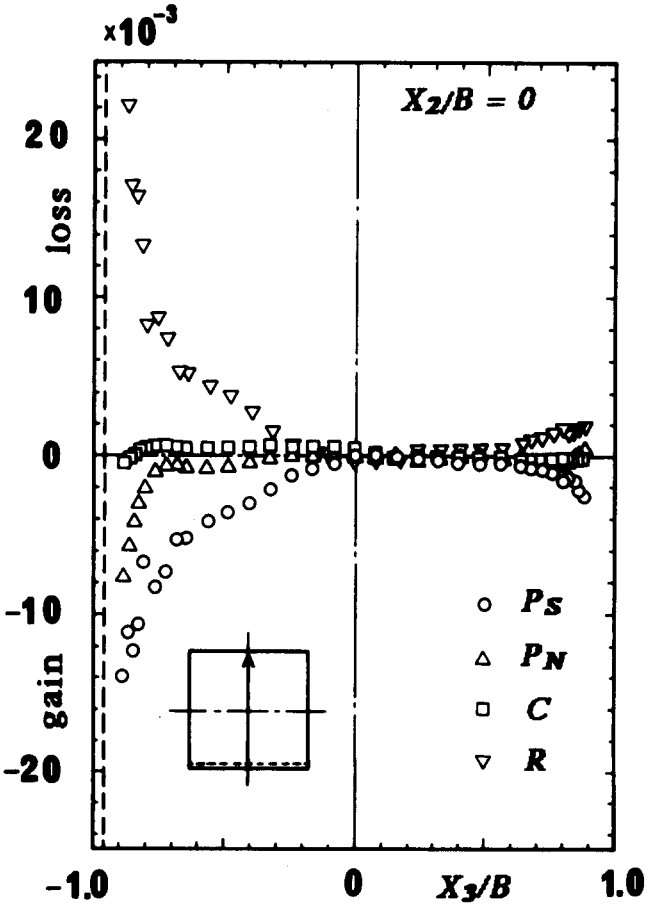

Figure 8 Energy balance for duct B

wall. Therefore, P_S, the product of $\overline{u_1 u_3}$ and $\partial U_1/\partial x_3$, becomes large in magnitude near the rough wall. Since station I is located near the flow reattachment point, $\partial U_1/\partial x_3$ would be very small immediately near the base plate of the rough wall. In the present experiment, however, the measurement point nearest to the wall (2.5 times the rib height from the wall) is located out of the separation bubble. Thus, the value of $\partial U_1/\partial x_3$ near the rough wall obtained in the present study is much larger than that near the smooth wall owing to the effective deceleration of U_1 by the ribs.

In the region near the rough wall in duct B, P_N is negative (gain in energy) and its value reaches nearly 60 percent of the value of P_S. It follows that, in contrast to the fact found in duct A, P_N makes a comparable contribution to P_S to the production of turbulence energy in this region. In the region immediate to the upper smooth wall, P_N is positive (loss in energy), but small, as opposed to being negative in the region near the rough wall. Detailed behavior of P_N is discussed in the next section.

The magnitude of the value of energy convection (term C) in duct B is much smaller than those of P_S and P_N. The contribution of the convection-to-energy balance, therefore, can be essentially neglected. This means that distortion in the contours of k does not necessarily coincide with the directions of the secondary flow vectors. On closer investigation, energy convection is negative from the center of the duct to the upper smooth wall, but is positive near the rough wall except in the close vicinity of the rough wall. The distribution of k shown in Figure 5 and the direction of secondary flow vectors along the x_3-axis explain this situation. Figure 9 is the secondary flow vector diagram obtained at station I and station II of duct B.[4,6] Secondary flow proceeds from the upper smooth wall along the x_3-axis toward the rough wall in duct B. It transports high energy fluid lumps near the smooth wall to the center of the duct and gives rise to a gain in turbulence energy near the duct center where the level of energy is relatively low. On the other hand, secondary flow transports low energy fluid lumps to the region near the rough wall where turbulence energy level is high. As a result, there is a loss of energy.

R, the sum of the dissipation term ε and the diffusion term D_f, has a large value near the rough wall as seen in Figure 8.

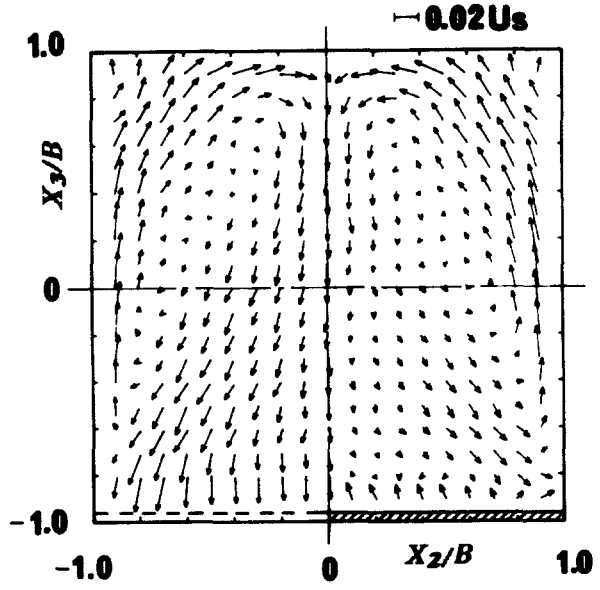

Figure 9 Secondary flow vector diagram for station I (left) and station II (right) of duct B

It follows that in this region the balance between $(P_S + P_N)$ and R has major effects on the distribution of k. In the central portion, R is almost equal to zero. This suggests that the loss caused by the dissipation is balanced with the gain caused by the diffusion.[14]

It is of much interest to compare the present results with the turbulence energy balance obtained in a two-dimensional (2-D) duct. Detailed experimental results have been presented by Hanjalic and Launder for turbulent flows through a 2-D duct with one rib-roughened wall.[14] In a central portion of their 2-D duct, there is a region in which the production by turbulent shear stress gives rise to a loss of energy. They attributed this "negative production" to diffusive transport of turbulent shear stress from the rough wall to the smooth wall. Although shear stress in duct B is diffused in the same direction as this 2-D duct, the negative production region (positive in values) is not observed in P_S distribution of duct B (Figure 8). This is attributed to the convective transport of turbulent shear stress caused by the secondary currents. On the symmetrical axis of duct B, shear stress is convected by the secondary currents from the upper smooth wall to the lower rough wall as expected from the left half of Figure 9. The direction of this convection is directly opposite to that of the diffusive transport mentioned previously. Therefore, the influence of the diffusion of shear stress on the energy production is cancelled by this convective transport. As described previously, the secondary flow does not influence decisively the distribution of the turbulence energy in the ducts. However, it plays an important role for establishing the local characteristics of the turbulence energy balance.

Contribution of turbulent normal stresses

Turbulence energy production caused by turbulent normal stresses is expressed in Equation 3c. The first term on the right-hand side of Equation 3c expresses the energy production caused by the primary flow velocity gradient in the direction of the primary flow. The value of this term is zero when the flow does not change in the x_1-direction. The second and third terms express the contributions of turbulent normal stresses and the secondary flow velocity gradients in the transverse directions. These two terms should be taken into account for those flows in noncircular ducts that are accompanied by the secondary flow of the second kind. In order to compare the contribution of each term in Equation 3c, the distribution of each term along the axis of symmetry of the duct is shown in Figures 10 and 11. In these figures, P_{Ni} $(i = 1, 2, 3)$ are defined as

$$P_{N1} = \overline{u_1^2}\frac{\partial U_1}{\partial x_1}\cdot\frac{D}{U_S^3}, \quad P_{N2} = \overline{u_2^2}\frac{\partial U_2}{\partial x_2}\cdot\frac{D}{U_S^3}, \quad P_{N3} = \overline{u_3^2}\frac{\partial U_3}{\partial x_3}\cdot\frac{D}{U_S^3} \tag{4}$$

In the smooth duct A, P_{N1} is nearly equal to zero everywhere along the x_3 axis as shown in Figure 10. This supports the assumption that the flow is fully developed globally in the x_1-direction at the measuring cross section. It is remarkable that near the top and bottom walls P_{N2}, the contribution of the normal stress component in the direction parallel to those walls, is negative (gain in energy).

In duct B (Figure 11), P_{N1} has a large negative value (gain in energy) near the rough wall at $x_3/B < -0.7$. This is brought about by the change in U_1 in the x_1-direction caused by repeated separation and reattachment of the flow at a rib and downstream from it. Since the primary flow is decelerated in the x_1-direction downstream of the rib (station I), $\partial U_1/\partial x_1$ is negative there, and therefore, P_{N1} becomes gain in energy. On approaching the upper smooth wall, P_{N1} tends to be zero, then becomes negative again, but finally turns positive (loss in

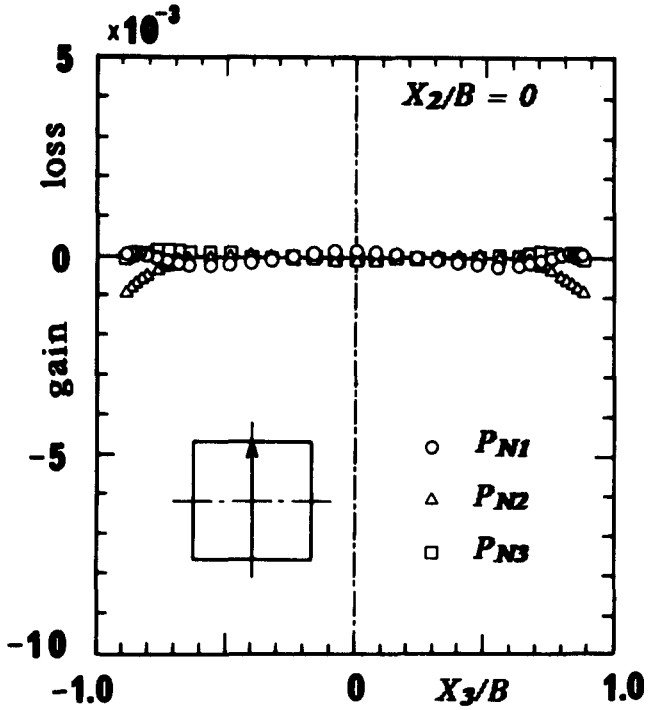

Figure 10 Energy production caused by normal stresses for duct A

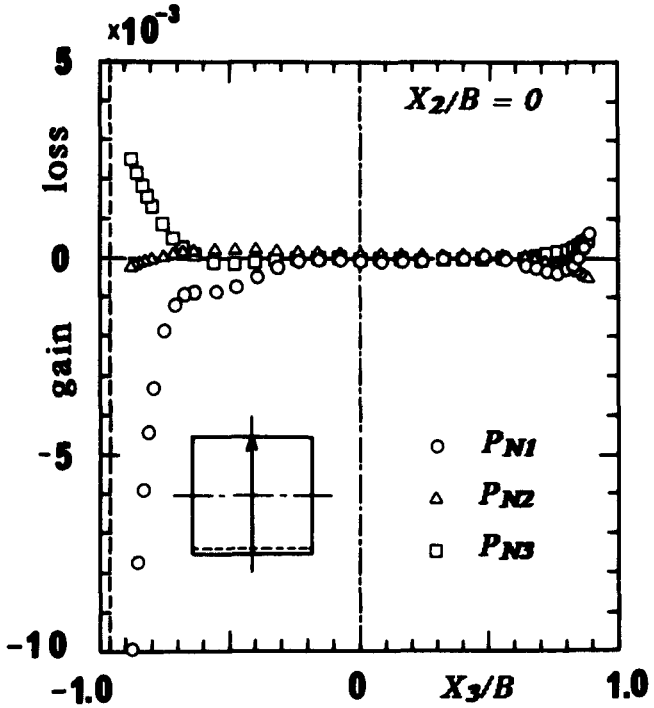

Figure 11 Energy production caused by normal stresses for duct B

energy) in the immediate vicinity of the upper wall. This shows that the effects of the streamwise change in the primary flow velocity appear near the upper smooth wall as well as near the rough wall.[15]

The magnitude of P_{N2}, energy production caused by the normal stress component in the direction parallel to the rough wall, is very small. It is negative near the walls, and near the rough wall it is almost the same as near the smooth wall. This shows that there are no remarkable effects of the rough wall on energy production caused by $\overline{u_2^2}$. Such a situation is recognized in the left half of Figure 9. The secondary flow vectors near the rough wall are directed almost perpendicularly to the rough wall over the wide range of x_2/B. As a result, the spanwise variation of U_2 and the resultant term P_{N2} becomes very small there. This fact means that the flow characteristics near the rough wall are quite similar to those of the 2-D boundary-layer flow over a rough surface.

On the other hand, P_{N3}, the production caused by the normal stress component in the direction normal to the rough wall, has a large positive value (loss in energy) near the rough wall, contrary to the negative values of P_{N1} and P_{N2}. This relatively large negative contribution of P_{N3} in station I comes from the acceleration of U_3 toward the rough wall, which is induced by the reattachment of the primary flow downstream of a rib. There is a region in which the value of P_{N3} is positive near the upper smooth wall, too.

When the rib-roughened wall is used as a heat transfer surface, the local maximum in the distribution of heat transfer coefficient is recognized at the flow reattachment point. This is attributed to high-level turbulence generated by the reattachment of the shear layer. For turbulent transport of heat, the fluctuating velocity component in the direction of maximum temperature gradient (u_3 for the rough wall in duct B) would be most effective. In the preceding experimental results, in fact, the values of $\overline{u_3^2}$ near the rough wall were about 2.8 times those observed near the smooth wall.[6] As a result of this high intensity of u_3, it is reported that the mean heat transfer coefficient on the rough wall becomes about 1.8 times that of the smooth wall.[16] The mechanism by which u_3 of high intensity is produced by the rough wall is explained as follows. As shown in Figures 5 and 11, P_S and P_{N1} (production of $\overline{u_1^2}$) brings about a large gain in turbulence kinetic energy. In contrast, P_{N3} (production of $\overline{u_3^2}$) becomes loss in energy at station I of duct B. Therefore, similar to the smooth duct, turbulence kinetic energy generated by $(P_S + P_{N1})$ is initially stored in $\overline{u_1^2}$ and then reidstributed to $\overline{u_2^2}$ and $\overline{u_3^2}$. The $\overline{u_3^2}$ redistributed from $\overline{u_1^2}$ is dissipated by the contribution of P_{N3} (sink term). This negative contribution of P_{N3} is disadvantageous to maintain high intensity of $\overline{u_3^2}$. The magnitude of P_{N3} can be effectively reduced, for example, by using a rib with a blunt trailing edge that makes the value of $\partial U_3/\partial x_3$ small.

The high level turbulence promotes the momentum exchange as well as the heat transfer. Therefore, it is expected that increase in the total flow resistance of the rib-roughened wall comes from not only the pressure drag caused by the separation bubbles behind the ribs but also the friction drag increased by the strong momentum exchange in the x_3 direction. In the preceding experiment, however, it was found that on the rib-roughened wall the pressure drag amounts to about 70 percent of the total flow resistance, and the value of the friction drag is almost the same as that of the smooth wall.[17] This result suggests the possibility that dissimilarity exists between the turbulent transport of heat and that of momentum. However, this should be discussed based on the $\overline{u_3 t}$- and the $\overline{u_1 u_3}$-equations, where t denotes fluctuation temperature, and this discussion is beyond the scope of the present paper.

The results stated in this section are obtained in the cross section downstream of the furthest downstream rib (station I in Figure 3). P_{N1}, the largest contributor in P_N, is brought about by the repetitive separation and reattachment of the primary flow. Therefore, there is a possibility of a change in P_N distributions depending on the relative streamwise location of the measurement cross section with respect to a rib. Hence, examinations of turbulence energy balance were carried out in the cross section atop a rib (station II in Figure 3) and discussed in the following section.

Distributions in cross section atop a rib (station II)

Examinations were carried out for duct B. The results are shown in Figures 12–14. Figure 12 shows the values of each term of Equation 4. It is remarkable that P_{N1} is positive (loss in energy) near a rib, opposite to negative values in station I (Figure 11). P_{N1} is positive at $x_3/B < -0.6$, which indicates that the effects of the ribbed wall on the flow extend as far from the wall as ten times the rib height. P_{N1} is positive, whereas P_{N3} is negative (gain in energy) near the rough wall. This is quite opposite to the results shown in Figure 11.

Such distributions of P_{N1} and P_{N3} in station II are explained qualitatively by considering the flow behavior near a rib. As schematically depicted in Figure 3, the primary flow is separated at the front edge of the rib and it is accelerated rapidly just above the rib.[11] This rapid acceleration of U_1 brings about a relatively large dissipative contribution (positive in sign) of P_{N1} near the rough wall. On the other hand, as observed in Figure 9b, U_3 becomes positive just above the rib owing to curvature of the streamlines. Over the entire portion on the x_3-axis except for the immediate vicinity of the rib, however, U_3 is negative, and therefore, $\partial U_3/\partial x_3$ and resultant production term P_{N3} become negative in sign near the rough wall.

The contribution of P_{N2} is relatively small in this cross section as similar as in station I. This also supports that the flow near the rib can be regarded as a 2-D boundary-layer flow.

In the vicinity of the upper smooth wall opposite to the rough wall, P_{N1} is negative as shown in Figure 12. This result is directly opposite to that shown in Figure 11, indicating that the effects of the difference in streamwise location of the measuring cross section are experienced not only in the region near the rough wall but also, though weak, near the smooth wall.

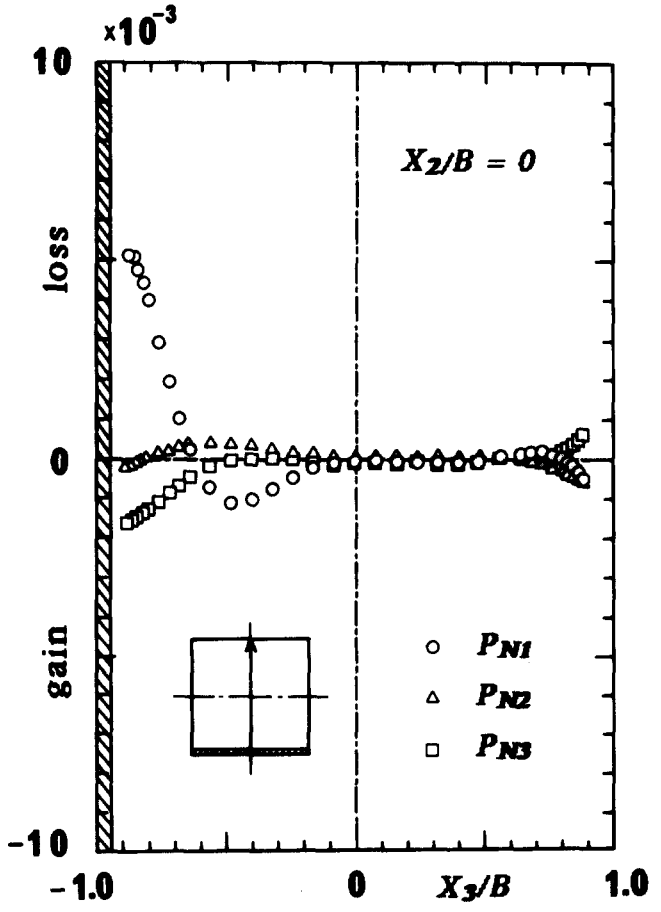

Figure 12 Energy production caused by normal stresses atop a rib for duct B

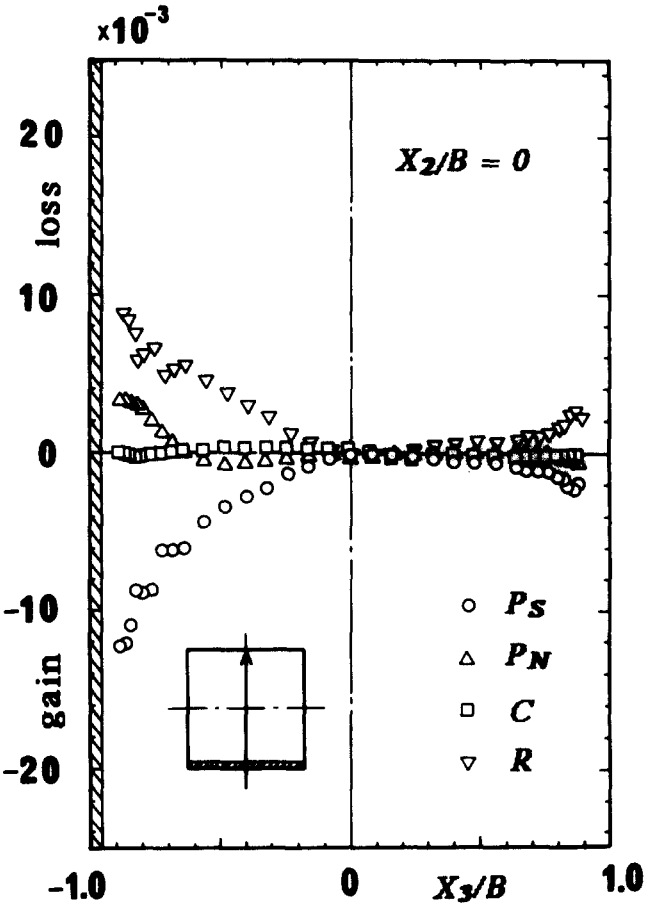

Figure 13 Energy balance atop a rib for duct B

Figure 13 shows the turbulence energy balances on the x_3-axis in station II. The distribution of P_S is qualitatively and quantitatively similar to that obtained in station I (Figure 8). However, as expected from Figure 12, P_N is positive (loss in energy) near the rough wall in contrast with its negative value in Figure 8. Therefore, as observed in the left half of Figure 14, the absolute values of $(P_S + P_N)$ in station II are less than half of those observed in station I as shown in Figure 5. This reduction of the energy production chiefly comes from dissipative contribution of P_{N1}. Near the rough wall in station II, the production of $\overline{u_1^2}$ expressed as $(P_S + P_{N1})$ amounts to only 30 percent of that observed in station I. The values of $\overline{u_1^2}$ in station II, however, were almost in the same level as those in station I. Similar result was obtained for distributions of $\overline{u_3^2}$, which are produced by the contribution of P_{N3}. Accordingly, as observed in the right half of Figure 14, the values of k obtained in station II are nearly on the same level as those in station I.

In order to explain the cause of the differences between the distributions of production terms and those of k, it is necessary to obtain the distribution of diffusion term D_f, in particular that of the pressure diffusion term. It is often reported, however, that accurate measurement of this term is very difficult at the present stage.[18] The problem remains to be solved in the future. Judging from the fact that there is little difference between the two contour maps of k obtained atop and downstream of the rib, the convection term $U_1\,\partial k/\partial x_1$ is expected to make little contribution to the turbulence energy balance, although its contribution was not considered in the present analysis.

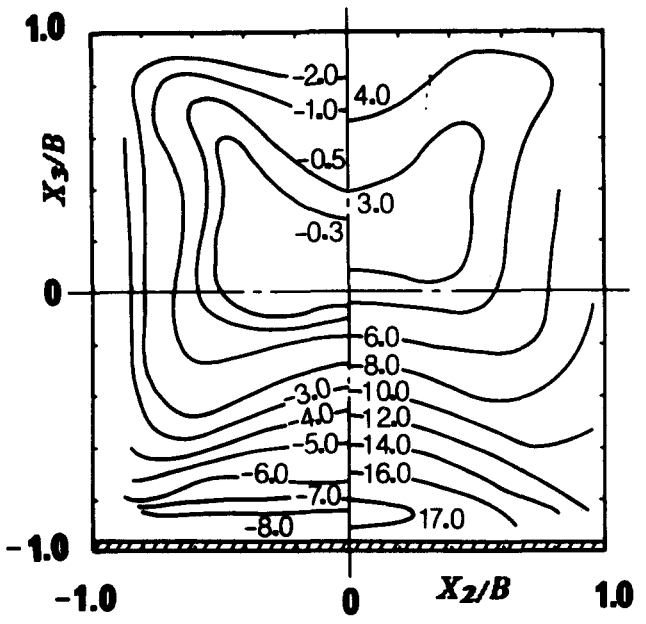

Figure 14 Turbulence energy production $(P_S + P_N) \times 10^3$ (left) and turbulence energy $k/U_S^2 \times 10^3$ (right) atop a rib for duct B

Concluding remarks

With due attention to the turbulence energy balances of the turbulent flows in square ducts with rough walls, we obtained the distributions of the production and convection of energy. Results obtained are summarized as follows:

(1) Turbulent shear stresses make the major contribution to the turbulence energy production both in smooth and rough ducts. Near the rough wall of the rough ducts, however, the contribution of the turbulent normal stresses and shear stresses are almost on the same level.

(2) Among the components of the energy production caused by the turbulent normal stresses, P_{N1} $(=\overline{u_1^2}\,\partial U_1/\partial x_1 \cdot D/U_S^3)$ makes the largest contribution. This is peculiar to the flow in ducts with rib-roughened walls. In the region near the rough wall, the contribution of P_{N3} $(=\overline{u_3^2}\,\partial U_3/\partial x_3 \cdot D/U_S^3)$, the production caused by the component normal to the rough wall, is also noticeable. The sign P_{N1} bears is opposite to that of P_{N3}, and their signs change depending on the relative streamwise locations of the cross section in relation to the rib; in station I (downstream of a rib), P_{N1} is negative (gain in energy) and P_{N3} is positive (loss in energy), but in station II (atop the rib), P_{N1} is positive and P_{N3} is negative.

(3) In both the smooth and the rough ducts, the amount of turbulence energy convected by the secondary flow is remarkably smaller than the amount of energy production. Consequently, the energy convection caused by the secondary flow has little effect on the turbulence energy balance in the ducts.

Acknowedgment

The authors express their thanks to Professor Shintaro Yamashita of Gifu University for his valuable advice. This research was supported by the Japanese Ministry of Education through a Grant-in-Aid for Scientific Research (Grant No. 63550163).

References

1 Han, J. C. Heat transfer and friction characteristics in rectangular channels with rib turbulators. *Trans. ASME J. Heat Transfer*, 1988, **110**, 321–328

2 Humphrey, J. A. C., and Whitelaw, J. H. Turbulent flow in a duct with roughness. In *Turbulent Shear Flows 2*, J. S. Bradbury et al., eds. Springer, Berlin, 1980, 174–188

3 Fujita, H., Yokosawa, H., Hirota, M., and Nagata, C. Fully developed turbulent flow and heat transfer in a square duct with two roughened facing walls. *Chem. Eng. Comm.*, 1988, **74**, 95–110

4 Fujita, H., Yokosawa, H., and Hirota, M. Secondary flow of the second kind in rectangular ducts with one rough wall. *Exp. Thermal Fluid Sci.*, 1989, **2**, 72–80

5 Yokosawa, H., Fujita, H., Hirota, M., and Iwata, S. Measurement of turbulent flow in a square duct with roughened walls on two opposite sides. *Int. J. Heat Fluid Flow*, 1989, **2**, 125–130

6 Fujita, H., Hirota, M., and Yokosawa, H. Experiments on turbulent flow in a square duct with a rough wall. In *Memoirs of the Faculty of Engineering, Nagoya University*, 1989, **41**, 154–168

7 Hinze, J. O. Secondary currents in wall turbulence. *Physics Fluids* Suppl., 1967, **10**, s122–s125

8 Hinze, J. O. Experimental investigation on secondary currents in the turbulent flow through a straight conduit. *Appl. Sci. Res.*, 1973, **28**, 453–465

9 Prandtl, L. *Führer durch die Strömungslehre*. Vieweg, Braunschweig, 1965, p. 221

10 Hinze, J. O. *Turbulence*, 2nd ed. McGraw-Hill, New York, 1975, 72

11 Hijikata, K., Ishiguro, H., and Mori, Y. Heat transfer augmentation in a pipe flow with smooth cascade turbulence promoters and its application to energy conversion, in *Heat Transfer in High Technology and Power Engineering*, W. J. Yang and Y. Mori, eds. Hemisphere, New York, 1987, 368–379

12 Liou, T. M., and Kao, C. F. Symmetric and asymmetric turbulent flows in a rectangular duct with a pair of ribs. *Trans. ASME, J. Fluids Eng.*, 1988, **110**, 373–379

13 Hirota, M., Fujita, H., and Yokosawa, H. Influence of velocity gradient on hot wire anemometry with an X-wire probe. *J. Physics E: Scientific Instruments*, 1988, **21**, 1077–1084

14 Hanjalic, K., and Launder, B. E. Fully developed asymmetric flow in a plane channel. *J. Fluid Mech.*, 1972, **51**, 301–335

15 Sparrow, E. M., and Tao, W. G. Enhanced heat transfer in a flat rectangular duct with streamwise-periodic disturbances at one principal wall. *Trans. ASME J. Heat Transfer*, 1983, **105**, 851–861

16 Han, J. C. Heat transfer and friction in channels with two opposite rib-roughened walls. *Trans. ASME, J. Heat Transfer*, 1984, **106**, 774–781

17 Furuya, Y., Miyata, M., and Fujita, H. Turbulent boundary layer and flow resistance on plate roughened by wires. *Trans. ASME, Ser. I, J. Fluids Eng.*, 1976, **98**, 635–644

18 Ramaprian, B., and Chandrasekhara, M. LDA measurements in plane turbulent jets. *Trans. ASME, J. Fluids Eng.*, 1985, **107**, 264–271